JEM Journal of Experimental Medicine

BRIEF DEFINITIVE REPORT

# SARS-CoV-2 induces human plasmacytoid predendritic cell diversification via UNC93B and IRAK4

Fanny Onodi[1], Lucie Bonnet-Madin[2], Laurent Meertens[2], Léa Karpf[1], Justine Poirot[1], Shen-Ying Zhang[3,4,5], Capucine Picard[4,6], Anne Puel[3,4,5], Emmanuelle Jouanguy[3,4,5], Qian Zhang[5], Jérôme Le Goff[1,7], Jean-Michel Molina[2,7], Constance Delaugerre[2,7], Jean-Laurent Casanova[3,4,5,8], Ali Amara[2], and Vassili Soumelis[1,9]

**Several studies have analyzed antiviral immune pathways in late-stage severe COVID-19. However, the initial steps of SARS-CoV-2 antiviral immunity are poorly understood. Here we have isolated primary SARS-CoV-2 viral strains and studied their interaction with human plasmacytoid predendritic cells (pDCs), a key player in antiviral immunity. We show that pDCs are not productively infected by SARS-CoV-2. However, they efficiently diversified into activated P1-, P2-, and P3-pDC effector subsets in response to viral stimulation. They expressed CD80, CD86, CCR7, and OX40 ligand at levels similar to influenza virus–induced activation. They rapidly produced high levels of interferon-α, interferon-λ1, IL-6, IP-10, and IL-8. All major aspects of SARS-CoV-2–induced pDC activation were inhibited by hydroxychloroquine. Mechanistically, SARS-CoV-2–induced pDC activation critically depended on IRAK4 and UNC93B1, as established using pDC from genetically deficient patients. Overall, our data indicate that human pDC are efficiently activated by SARS-CoV-2 particles and may thus contribute to type I IFN–dependent immunity against SARS-CoV-2 infection.**

## Introduction

Severe acute respiratory syndrome–coronavirus-2 (SARS-CoV-2) is the third zoonotic coronavirus that emerged in the last two decades. SARS-CoV-2 is the causative agent of coronavirus disease 2019 (COVID-19), which appeared in late 2019 in Wuhan, Hubei province in China (Keni et al., 2020; Tay et al., 2020). SARS-CoV-2 became rapidly pandemic; infections have now been detected in 216 countries and territories, and it is responsible for ∼46 million confirmed cases and >1 million deaths (World Health Organization, 2020). SARS-CoV-2 infection may lead to a diversity of clinical presentations, ranging from asymptomatic or mild "flu-like" syndrome in >98% of patients to severe and sometimes life-threatening acute respiratory failure in <2% of infected individuals (Tang et al., 2020). Disease aggravation usually occurs 8–10 d following initial symptoms (Tang et al., 2020). At this late stage, three main factors were shown to correlate with the progression and severity of the infection (Tang et al., 2020): (1) viral persistence was evidenced in the lung and systemic circulation, although it is not constant (Tang et al., 2020); (2) an excess production was seen of pro-inflammatory cytokines, such as IL-1β and IL-6 (Tay et al., 2020); and (3) there was a defect in type I IFN production, especially in critically ill patients (Tay et al., 2020; Acharya et al., 2020). Whether an imbalance between inflammatory cytokines and type I IFN occurs early in the disease, at the stage of the primary infection, and whether the virus itself may be responsible are currently unknown. More recent studies clarified the pathogenesis of life-threatening COVID-19 pneumonia in ∼15% of patients. While some patients carry inborn errors of TLR3- and IRF7-dependent type I IFN production and amplification (Zhang et al., 2020b), at least 10% of patients have preexisting neutralizing

[1]Université de Paris, Institut de Recherche Saint-Louis, Institut National de la Santé et de la Recherche Médicale U976, Hôpital Saint-Louis, Paris, France; [2]Université de Paris, Institut de Recherche Saint-Louis, Institut National de la Santé et de la Recherche Médicale U944, Centre National de la Recherche Scientifique 7212, Hôpital Saint-Louis, Paris, France; [3]Laboratory of Human Genetics of Infectious Diseases, Necker Branch, Institut National de la Santé et de la Recherche Médicale, Necker Hospital for Sick Children, Paris, France; [4]Université de Paris, Institut National de la Santé et de la Recherche Médicale Unite Mixte de Recherche 1163, Institut Imagine, Paris, France; [5]St. Giles Laboratory of Human Genetics of Infectious Diseases, Rockefeller Branch, The Rockefeller University, New York, NY; [6]Study Center for Primary Immunodeficiencies, Necker Hospital for Sick Children, Assistance Publique–Hôpitaux de Paris, Paris, France; [7]Laboratoire de Virologie et Département des Maladies Infectieuses, Hôpital Saint-Louis, Assistance Publique–Hôpitaux de Paris, Paris, France; [8]Howard Hughes Medical Institute, New York, NY; [9]Assistance Publique-Hôpitaux de Paris, Hôpital Saint-Louis, Laboratoire d'Immunologie, Paris, France.

Correspondence to Vassili Soumelis: vassili.soumelis@aphp.fr; Ali Amara: ali.amara@inserm.fr.

auto-antibodies to type I IFNs (Bastard et al., 2020). These studies suggested that the pathogenesis of life-threatening COVID-19 proceeds in two steps, with defective type I IFNs in the first days of infection unleashing excessive inflammation from the second week onward (Zhang et al., 2020a).

Investigating the early innate immune response to SARS-CoV-2 is essential both to understand the mechanisms underlying an efficient viral control and to shed light on possible subsequent life-threatening complications. Plasmacytoid predendritic cells (pDCs) play a particularly important role as the major source of type I IFN in response to viral infection due to their constitutively high levels of IRF7 expression (Liu, 2005). pDCs can sense a large array of viruses including the coronaviruses SARS-CoV, murine hepatitis virus, and the Middle East respiratory syndrome coronavirus (MERS; Cervantes-Barragan et al., 2007, 2012; Raj et al., 2014; Scheuplein et al., 2015). pDCs recognize MERS through TLR7 (Scheuplein et al., 2015). They respond to viruses by producing innate cytokines, including all forms of type I IFNs (α and β), type III IFN, and inflammatory cytokines, in particular TNF-α and IL-6 (Liu, 2005; Gilliet et al., 2008). However, different viruses may induce different cytokine patterns (Thomas et al., 2014), possibly creating an imbalance between IFN versus inflammatory cytokine response. Additionally, some viruses were shown to subvert pDC functions through different mechanisms not necessarily related to productive infection. This is the case for human immunodeficiency virus, which may induce pDC apoptosis in vitro (Meyers et al., 2007) and pDC depletion in vivo (Soumelis et al., 2001; Meera et al., 2010). Human hepatitis C virus can inhibit IFN-α production by pDCs through the glycoprotein E2 binding to BDCA-2 (Florentin et al., 2012). Human papillomavirus induces very low IFN response in pDCs (Bontkes et al., 2005), which may be due to impaired TLR7 and TLR9 signaling (Hirsch et al., 2010). Whether SARS-CoV-2 induces efficient pDC activation or may interfere with various biological pathways in pDCs is currently unknown.

## Results and discussion

### SARS-CoV-2 induces activation and diversification of primary human pDCs

To efficiently recapitulate SARS-CoV-2–pDC interactions, we used two strains of SARS-CoV-2 primary isolates. Their viral genome sequences were nearly identical, with 99.98% identity. Sequence comparison with reference strain Wuhan-Hu-1 (National Center for Biotechnology Information GenBank accession no. NC_045512.2) showed that both strains contain a subset of mutations (C241T, C30307T, A23403G, and G25563T), characteristic of the GH clade based on Global Initiative of Sharing All Influenza Data nomenclature. Human primary pDCs were purified from healthy donor peripheral blood mononuclear cells (PBMCs) by cell sorting. First, we asked whether SARS-CoV-2 was able to induce pDC activation and diversification into IFN-producing and/or T cell–stimulating effectors, as we previously described for influenza virus A (Flu; Alculumbre et al., 2018). After 24 h of culture, SARS-CoV-2–activated pDCs efficiently diversified into P1 (PD-L1$^+$CD80$^-$), P2 (PD-L1$^+$CD80$^+$), and P3 (PD-L1$^+$CD80$^+$) pDC subsets, similar to Flu stimulation (Fig. 1 A). P1-, P2-, and P3-pDCs were all significantly induced by SARS-CoV-2 and Flu as compared with medium control (Fig. 1 B). In parallel, we observed a sharp decrease in nonactivated P0-pDCs (PD-L1$^-$CD80$^-$; Fig. 1, A and B). SARS-CoV-2–induced pDC activation was comparable with magnetically versus FACS-sorted pDCs (Fig. S1, A and B), confirming that both methods are suitable for subsequent experiments. All main findings were confirmed on at least three independent experiments using FACS-sorted pDCs, with a protocol that excluded AS-DC, a rare dendritic cell (DC) subset that shares some markers and functional features with pDCs (Villani et al., 2017), based on CD2, CD5, and AXL expression (Fig. S1 A). pDC activation and diversification were observed with two independent primary SARS-CoV-2 strains (Fig. 1 C), which both induced similar proportions of P1-P3 subsets. pDC diversification was also observed by co-culturing of pDCs with SARS-CoV-2–infected Vero E6 cells with a similar efficiency to free SARS-CoV-2 (Fig. S1 C). SARS-CoV-2 improved pDC viability as compared with medium condition (Fig. 1 D), which is compatible with subsequent effector functions.

The fact that SARS-CoV-2 induced a complete diversification into the three activated pDC subsets suggests that different aspects of pDC-mediated immunity are engaged following viral challenge: type I IFN production and innate immunity mediated by P1-pDCs, T cell stimulation mediated by P3-pDCs, and a mixed innate and adaptive effector function through P2-pDCs (Alculumbre et al., 2018). Such a strong innate immune response could be central to the systemic and local inflammatory manifestations in primary symptomatic SARS-CoV-2 infection (Asselah et al., 2020).

### Human pDCs are not productively infected by SARS-CoV-2

Next, we asked whether SARS-CoV-2–induced pDC activation was dependent on productive infection. We first checked whether pDCs express at their cell surface ACE2, the major SARS-CoV-2 entry receptor (Hoffmann et al., 2020). No significant expression was detected using an anti–ACE2-specific antibody, as compared with a low and high expression on Vero E6 and 293T-ACE2 cell lines, respectively (Fig. 1 E). The ability of pDCs to replicate SARS-CoV-2 was then assessed. Human pDCs were challenged with SARS-CoV-2 strain 220_95 at a multiplicity of infection (MOI) of 2, and cultured for 2 h, 24 h, or 48 h. Our results showed that pDCs were refractory to SARS-CoV-2 infection, as evaluated by quantifying (1) the intracellular production of the nucleoprotein antigen (Fig. 1 F), or the accumulation of viral RNA in SARS-CoV-2–infected cells (Fig. S1 D); and (2) the release of infectious progeny virus in the supernatants of infected cells using plaque assays (Fig. 1 G). As positive control, the permissive Vero E6 cells produced high level of the nucleoprotein antigen, increased viral RNA overtime (Fig. S1 D), and high viral titers following SARS-CoV-2 incubation (Fig. 1 G). Similar results were obtained with pDCs isolated from three independent donors (Fig. S1 E). Overall, these results show that pDCs are resistant to SARS-CoV-2 infection and are efficiently activated by the virus independently of ACE2 expression. Their viability was not affected by SARS-CoV-2 challenge.

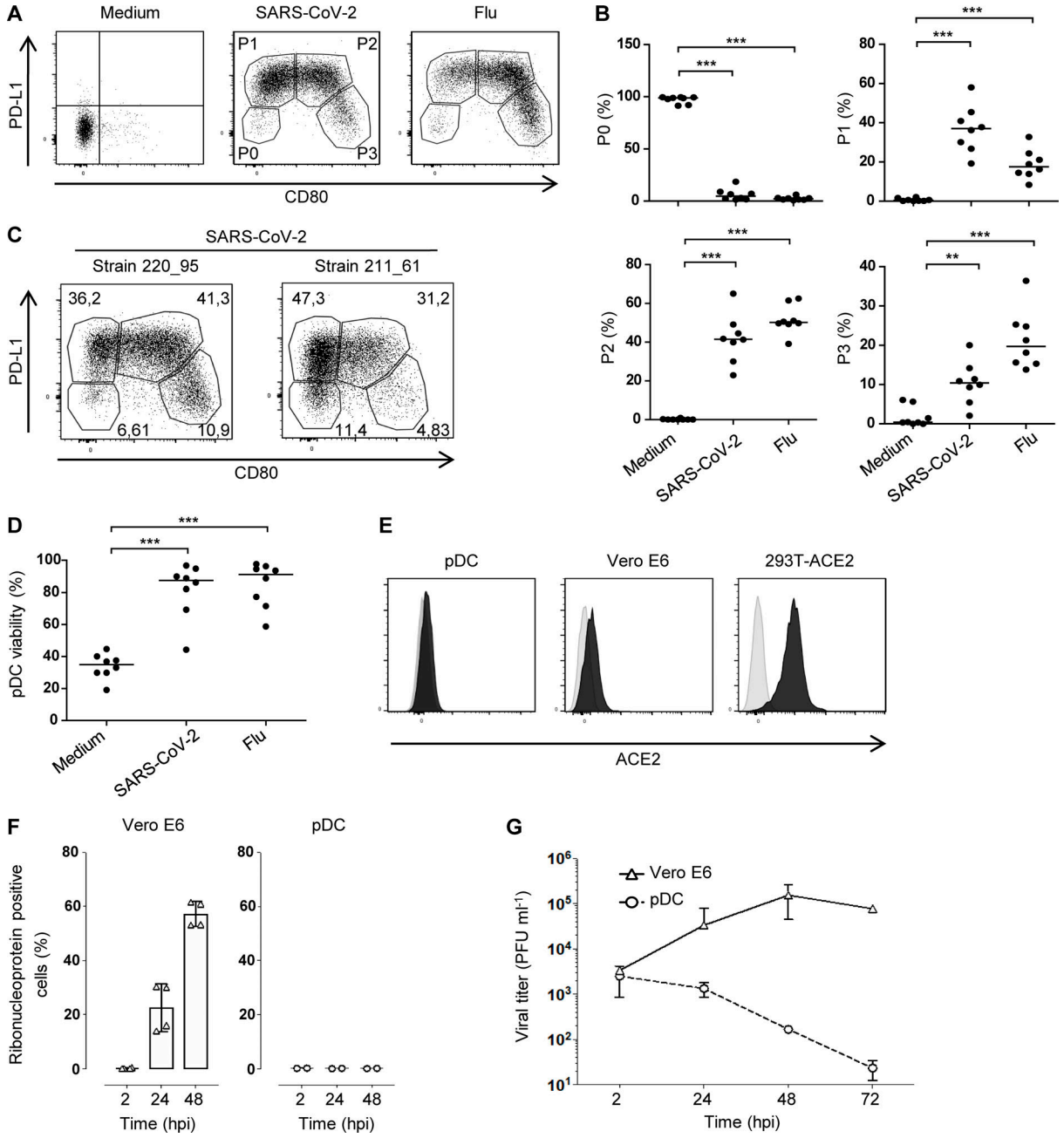


Figure 1. **SARS-CoV-2 induces activation and diversification of primary human pDCs.** Sorted blood pDCs from healthy donors were cultured for 24 h with medium, SARS-CoV-2, or Flu. **(A)** Dot plot showing pDC activation and diversification through the expression of PD-L1 and CD80 into P1, P2, and P3 subpopulations. Results from one healthy donor representative of $n = 8$. **(B)** Quantification of the three populations. Bars represent medians of $n = 8$ healthy donors from six independent experiments. **(C)** Dot plot showing pDC activation from different strains of SARS-CoV-2 isolated from two patients. Results from one healthy donor representative of $n = 3$. **(D)** Percentage of live pDCs after 24 h of culture with medium, SARS-CoV-2, or Flu. $n = 8$ healthy donors from six independent experiments. **(E)** Histogram of ACE2 expression on pDCs, Vero E6, and 293T-ACE2 (black) compared with the isotype (light gray). Results from one experiment representative of $n = 3$. **(F)** Intracellular production of SARS-CoV-2 ribonucleoprotein in Vero E6 and pDCs at 2, 24, or 48 h post-infection (hpi) with SARS-CoV-2. Results from one experiment representative of $n = 3$. **(G)** Infectious viral titers in the supernatants of SARS-CoV-2–infected Vero E6 and pDCs at 2, 24, 48, or 72 hpi. Results from one experiment representative of $n = 3$. **, $P < 0.01$; ***, $P < 0.005$; Mann–Whitney test.

### Upregulation of major immune checkpoints on SARS-CoV-2–activated pDC

Activating immune checkpoints play a key role in T cell stimulation, and serve as surrogate markers of DC differentiation (Guermonprez et al., 2002). We first assessed the dose-dependent effect of SARS-CoV-2 on CD80 expression and subset diversification. CD80 was induced in a dose-dependent manner by SARS-CoV-2 at MOI 0.04–1 (Fig. 2 A). This was accompanied by an increase in the P3-pDC subset and a slight decrease in P1-pDCs (Fig. 2 B). A detailed phenotypic analysis was subsequently performed on pDCs after 24 and 48 h of culture with SARS-CoV-2 (Fig. 2 C and Fig. S2 A). Diversification was observed at both time points, with a

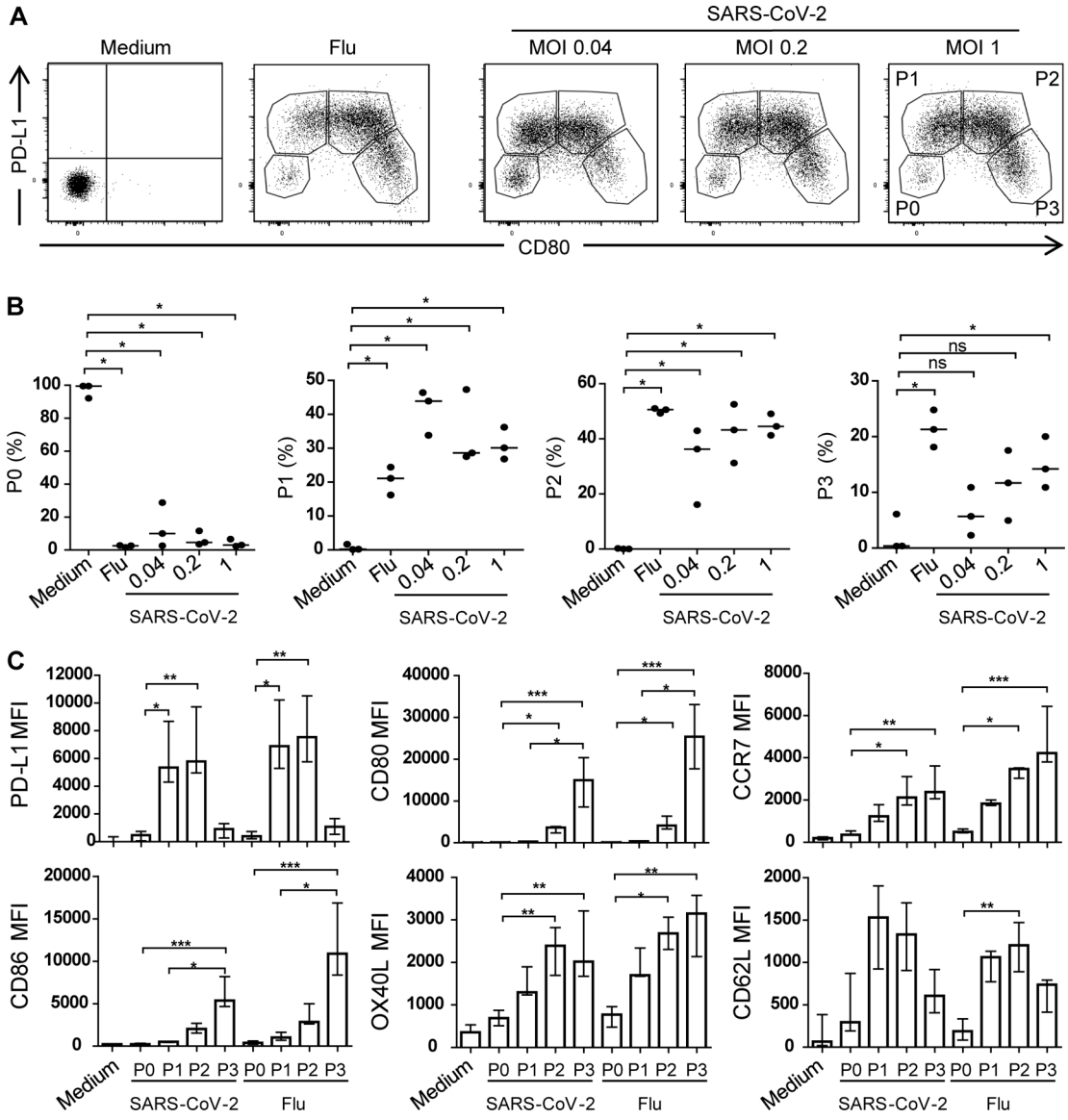


Figure 2. **SARS-CoV-2 induces pDC activation in a dose-dependent manner.** Sorted blood pDCs from healthy donors were cultured for 24 h with medium, Flu, or SARS-CoV-2 at an MOI of 0.04, 0.2, or 1. **(A)** Dot plot showing pDC activation through the expression of PD-L1 and CD80. Results from one healthy donor representative of $n = 3$. **(B)** Quantification of the three populations. Bars represent medians of $n = 3$ healthy donors from three independent experiments. **(C)** pDC geometric mean (mean fluorescence intensity [MFI]) of activation markers after 24 h of culture with medium, Flu, or SARS-CoV-2 at an MOI of 1. Histograms represent medians and bars interquartile ranges of $n = 5$ healthy donors from three independent experiments. *, $P < 0.05$; **, $P < 0.01$; ***, $P < 0.001$; Mann–Whitney test (B); Kruskal–Wallis with Dunn's multiple comparisons posttest (C). ns, not significant.

slight increase in P3-pDCs at 48 h (Fig. S2 A). P2- and P3-pDCs significantly upregulated CD80, CD86, CCR7, and OX40L, as compared with nonactivated P0-pDCs, in both SARS-CoV-2 and Flu conditions (Fig. 2 C). PD-L1 and CD62L, an integrin that promotes lymph node homing, were both higher on P1- and P2-pDCs (Fig. 2 C). Expression of checkpoint molecules persisted at 48 h, especially the higher CD80 and CD86 expression on P3-pDCs (Fig. S2 B).

### Efficient production of type I and type III IFNs by SARS-CoV-2–activated pDCs

A key and defining function of pDCs is their ability to produce large amounts of type I IFN, driven by their constitutively high levels of IRF7 (Liu, 2005). We measured the production of several cytokines at the protein level after 24 h of culture. Both SARS-CoV-2 and Flu induced high levels of IFN-α2 and IFN-λ1, both being critical antiviral effector cytokines (Fig. 3 A). IFN-α2 levels following SARS-CoV-2 activation reached up to 80 ng/ml, indicating a very efficient activation. The chemokine IP-10 was also significantly induced (Fig. 3 A), possibly due to an autocrine IFN loop (Blackwell and Krieg, 2003). Inflammatory cytokines IL-6 and IL-8 were comparably induced by SARS-CoV-2 and Flu (Fig. 3 A). However, TNF-α levels were marginally induced by SARS-CoV-2 when compared with Flu activation (Fig. 3 A). Cytokine production was maintained after 48 h of viral activation (Fig. S2 C). Secreted protein levels were similar to 24 h levels for most cytokines.

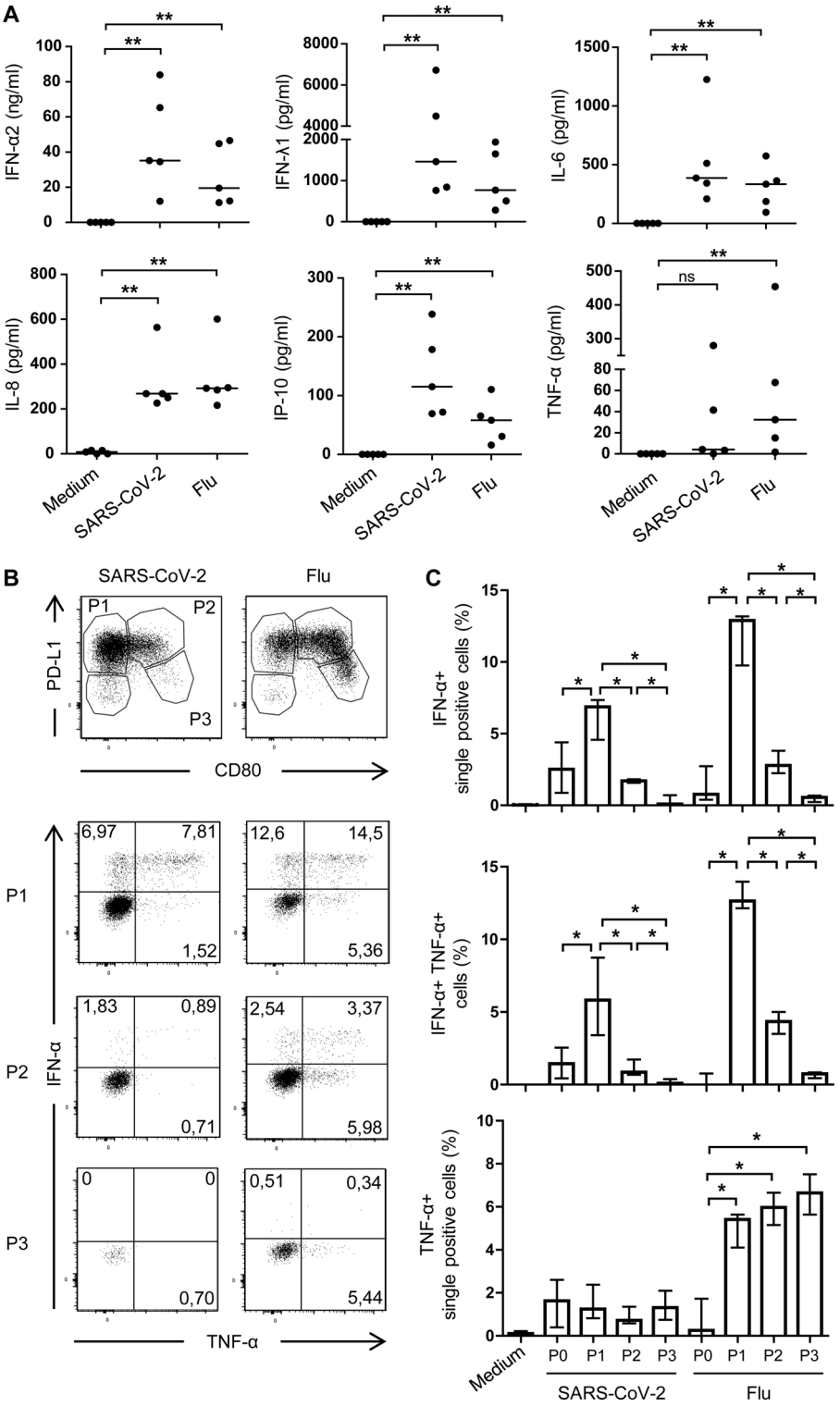


Figure 3. **SARS-CoV-2–activated pDCs produce pro-inflammatory cytokines.** Sorted blood pDCs from healthy donors were cultured for 24 h with medium, Flu, or SARS-CoV-2. **(A)** Quantification of secreted pro-inflammatory cytokines after 24 h of culture. Bars represent medians of $n$ = 5 healthy donors from three independent experiments. **(B)** Dot plot showing pDC activation through the expression of PD-L1 and CD80 (upper plots), and intracellular IFN-α and TNF-α in P1, P2, or P3 populations (lower plots). Results from one healthy donor representative of $n$ = 4. **(C)** Percentages of IFN-α single-positive, IFN-α$^+$ TNF-α$^+$ double-positive, and TNF-α single-positive cells in P0, P1, P2, or P3 populations. Histograms represent medians and bars interquartile ranges of $n$ = 4 healthy donors from three independent experiments. *, P < 0.05; **, P < 0.01; Mann–Whitney test. ns, not significant.

Interestingly, IFN-α levels rose by threefold between 24 h and 48 h for one donor (Fig. 3 A and Fig. S2 C), indicating the possibility of increased production. Such a strong IFN producer suggests a potential virus controller.

We have shown that P1-, P2-, and P3-pDCs exhibit different functions in response to Flu activation, including different cytokine profiles (Alculumbre et al., 2018). We questioned whether this functional specialization was similar following SARS-CoV-2 challenge. pDCs were cultured with either Flu or SARS-CoV-2 for 24 h, and P1-, P2-, and P3-pDC differentiation was assessed, along with intracellular IFN-α and TNF-α staining (Fig. 3 B). In the SARS-CoV-2 condition, IFN-α was essentially produced by P1- and to a lower extent by P2-pDCs, with 12% and 3% of IFN-α positive cells, respectively. TNF-α was also mainly produced by P1-pDCs, with 7% expressing cells (Fig. 3, B and C). P3-pDCs produced very few cytokines. Similar results were observed

following Flu challenge (Fig. 3 C). These data showed that IFN-α and TNF-α production are features of P1-pDCs, as well as P2-pDCs, and that SARS-CoV-2 induces a functional specialization of pDC subsets, similar to Flu.

Because the oropharyngeal mucosa is an entry site for SARS-CoV-2, we aimed at validating our results using pDCs purified from tonsils. SARS-CoV-2 induced a marked diversification of tonsillar pDCs into all three activated subsets (Fig. S2 D). Tonsillar pDC efficiently produced IFN and inflammatory cytokines in response to SARS-CoV-2 (Fig. S2 E). Overall, our results establish SARS-CoV-2 as a very efficient inducer of type I and type III IFN responses. Inflammatory cytokines were induced at similar level as Flu activation, without any significant imbalance that would be suggestive of excessive inflammatory response.

### SARS-CoV-2–induced pDC activation is inhibited by hydroxychloroquine (HCQ)

We then asked whether pharmacological agents could modulate pDC diversification and cytokine production. HCQ is known to inhibit endosomal acidification, which may diminish pDC activation (Sacre et al., 2012). Additionally, it is being tested in several clinical studies as a potential treatment for COVID-19 (Das et al., 2020). Hence, we addressed its role in SARS-CoV-2–induced pDC activation. Following 24 h of culture, we found that HCQ inhibited pDC diversification in response to SARS-CoV-2, which is similar to the decrease observed with Flu, used as a positive control (Fig. 4 A). In particular, P2- and P3-pDC differentiations were almost completely inhibited (Fig. 4 B). Inhibition of SARS-CoV-2–induced pDC diversification by HCQ was dose-dependent (Fig. S3 A). The significant decrease in P3-pDCs was paralleled by a decrease in CD80, CD86, and CCR7 expression (Fig. 4, C and D). OX40-ligand expression was not significantly affected by HCQ (Fig. 4, C and D). However, HCQ inhibited the appearance of an OX40-ligand$^{high}$ pDC population (Fig. S3, B and C), which may impact subsequent T cell activation. Last, we assessed the effect of HCQ on innate pDC functions. We measured cytokine production after 24 h of SARS-CoV-2–induced pDC activation in the presence or absence of HCQ. We found that IFN-α and -λ levels were decreased by HCQ (Fig. 4 E). This was also the case for IL-6 and IL-8, with a much lesser impact on IP-10 (Fig. 4 E). Together, these results show that HCQ inhibits SARS-CoV-2–induced pDC diversification and cytokine production.

### pDC response to SARS-CoV-2 depends on IRAK4 and UNC93B1

To gain mechanistic insights, we took advantage of studying pDCs from patients with genetic deficiencies in the TLRs signaling pathway (Rothenfusser et al., 2002; Casanova et al., 2011). While pDCs do not express detectable TLR3, they express TLR7 and TLR9 (Liu, 2005). We investigated pDCs from patients homozygous for germline mutations, resulting in loss of function of IRAK4 (one patient), which with MyD88 is required for signaling of IL-1Rs and TLRs other than TLR3 (Frazão et al., 2013), or UNC93B1 (two patients), which is required for signaling of endosomal TLR3, TLR7, TLR8, and TLR9 (Picard et al., 2003; Casrouge et al., 2006; Lee and Barton, 2014). pDCs from one TLR3-deficient patient was used as negative control (Zhang et al., 2007; Guo et al., 2011; Fig. 5). pDCs from IRAK4- and UNC93B1-deficient patients did not diversify into P1, P2, and P3 activated subpopulations when compared with healthy donors (Fig. 5 A). This lack of diversification was associated with a complete absence of IFN-α2, IP-10, and IL-6 secretion, establishing a critical role of these molecular nodes in SARS-CoV-2 activation of pDCs (Fig. 5 B). On the contrary, TLR3 deficiency did not significantly impact SARS-CoV-2–induced pDC activation, associated with diversification, and secretion of antiviral cytokines (Fig. 5, A and B). Taken together, these results identify IRAK4 and UNC93B1 as two critical players in controlling SARS-CoV-2 pDC activation.

In this study, we have analyzed the interaction between primary SARS-CoV-2 isolates and human primary pDCs. Our results demonstrate that SARS-CoV-2 is a strong IFN inducer by efficiently stimulating primary pDCs. Both type I and type III IFNs were induced at high levels in P1-pDCs upon SARS-CoV-2 stimulation. This strongly suggests that the defects observed in critically ill COVID-19 patients are acquired during disease evolution through secondary events, not necessarily associated with direct effects of the virus. Possible mechanisms could be related to inflammatory cytokines, such as TNF, and the endogenous glucocorticoid response, with both able to promote pDC apoptosis (Abe and Thomson, 2006; Lepelletier et al., 2010).

Our results are consistent with those obtained using other coronaviruses, such as SARS-CoV (Cervantes-Barragan et al., 2007), MERS (Raj et al., 2014), and murine hepatitis virus (Cervantes-Barragan et al., 2007, 2012), which all induced an efficient IFN response by pDCs independently of viral replication. However, pDC response to MERS depended on binding to its receptor DPP4 (Raj et al., 2014). In our study, viral sensing was independent of the expression of the ACE2 entry receptor. Importantly, pDC response to SARS-CoV-2 was dependent on two critical molecular components downstream of TLRs, IRAK4 and UNC93B1. These results are consistent with studies showing the importance of IRAK4 in pDC response to immune complexes through TLR7 (Hjorton et al., 2018; Corzo et al., 2020). UNC93B1 was reported to regulate transport, stability, and function of endosomal TLR3, TLR7, TLR8, and TLR9 (Lee and Barton, 2014). Our studies are also consistent with our previous studies of pDCs in patients with inherited IRF7 deficiency (Ciancanelli et al., 2015; Zhang et al., 2020b). Indeed, we showed that IRF7-deficient pDCs did not produce type I IFNs other than IFN-β in response to influenza virus or SARS-CoV-2 (Zhang et al., 2020b). In our study, we provide direct evidence for a specific role of UNC93B1 in primary human pDCs. With the only shared features of human IRAK4 and UNC93B deficiencies their control of cellular responses to TLR7, TLR8, and TLR9 (Casanova et al., 2011), we can infer from these studies that human pDCs recognize SARS-CoV-2 via one or another of them, or a combination thereof. The abundant expression of TLR7 on human pDCs suggests that this receptor may play an important role in this process (Gilliet et al., 2008; van der Made et al., 2020). It will be important to analyze the natural history of SARS-CoV-2 infection in patients with inborn errors of the TLR7, TLR8, and

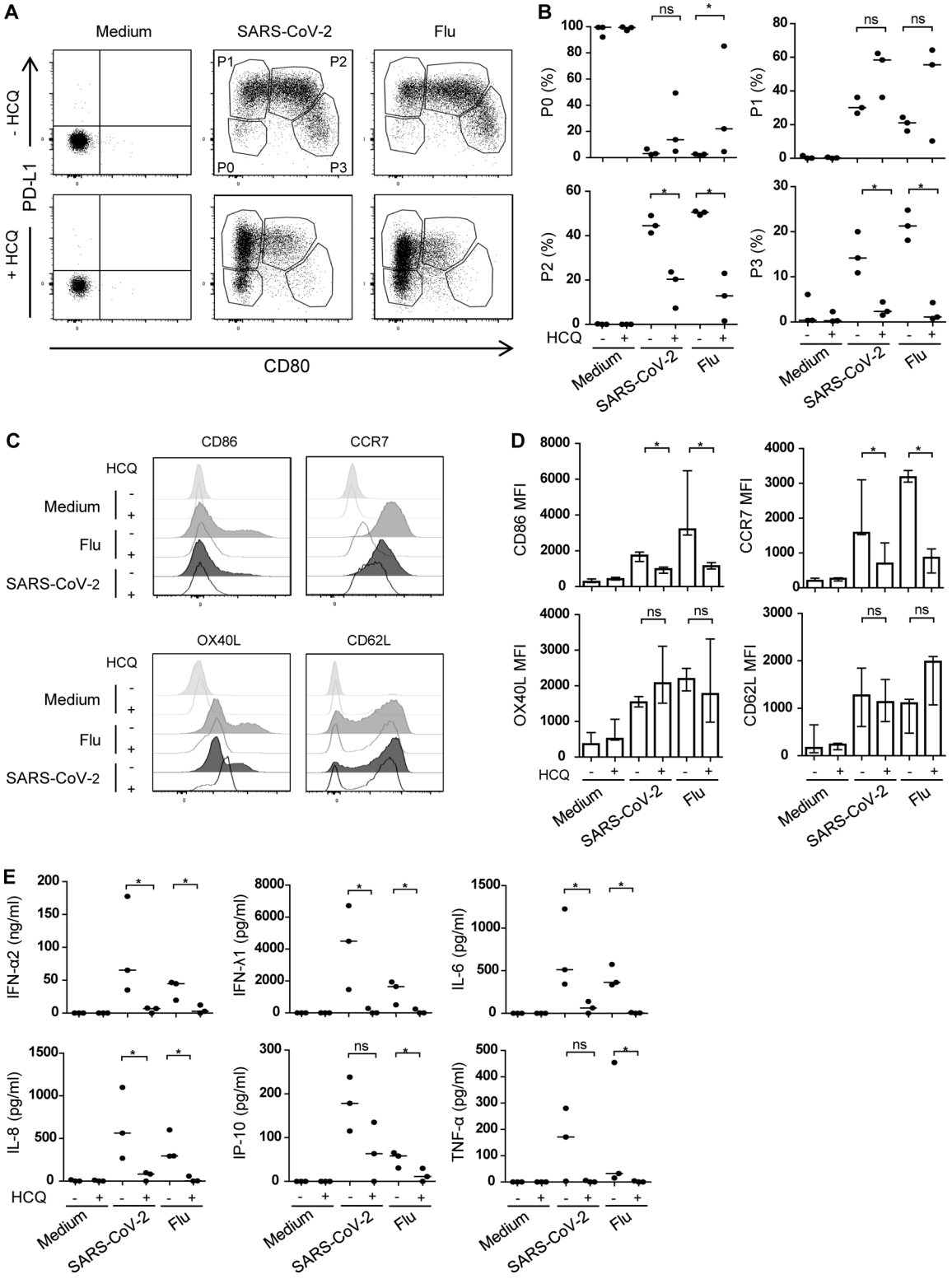


Figure 4. **SARS-CoV-2–induced pDC activation is inhibited by HCQ.** Sorted blood pDCs from healthy donors were cultured for 24 h with medium, Flu, or SARS-CoV-2 at an MOI of 1 with or without the presence of HCQ. **(A)** Dot plot showing pDC diversification in P1, P2, and P3 subpopulations in the presence of HCQ. Results from one healthy donor representative of $n = 3$. **(B)** Quantification of the three populations. Bars represent medians of $n = 3$ healthy donors from three independent experiments. **(C)** Histograms of pDCs' activation markers. Results from one healthy donor representative of $n = 3$. **(D)** Geometric mean (mean fluorescence intensity [MFI]) of activation markers. Histograms represent medians and bars interquartile ranges of $n = 3$ healthy donors from three independent experiments. **(E)** Quantification of pro-inflammatory cytokines production. Bars represent medians of $n = 3$ healthy donors from three independent experiments. *, $P < 0.05$; Mann–Whitney test. ns, not significant.

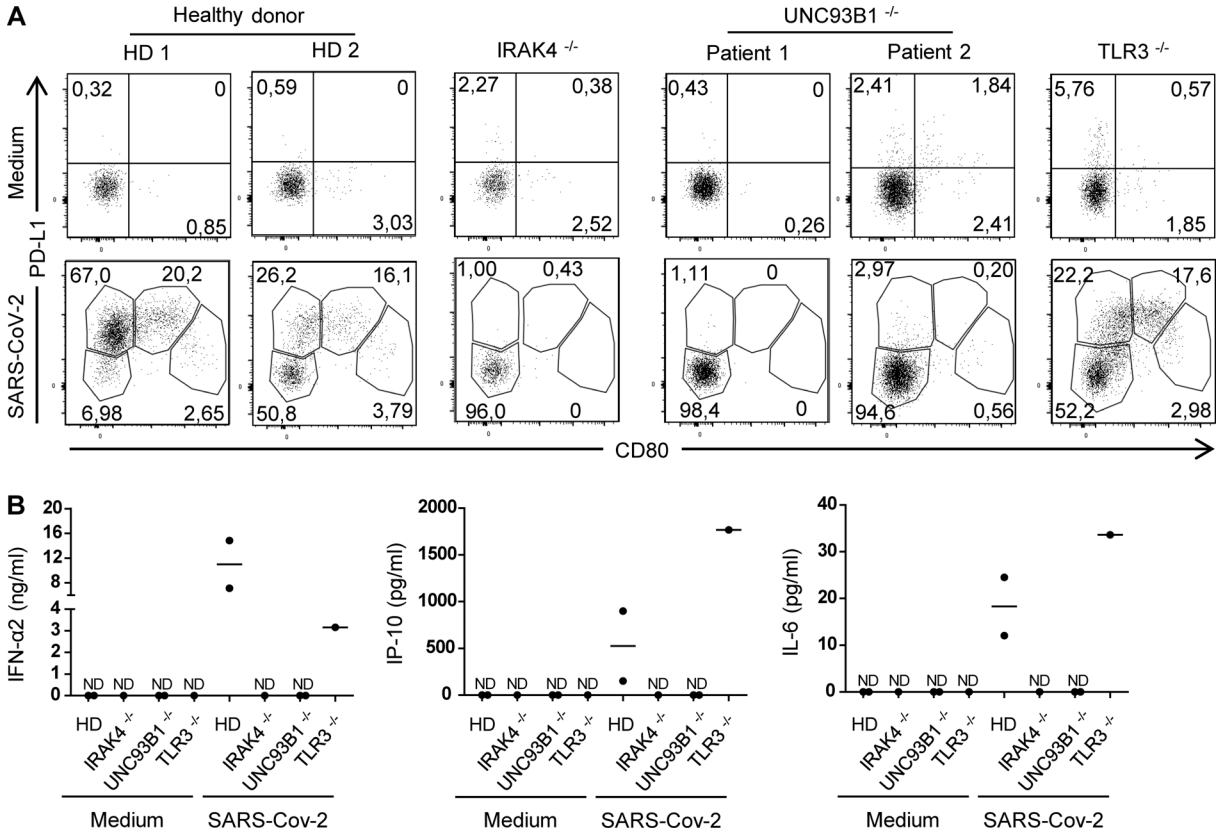


Figure 5. **SARS-CoV-2–induced pDC activation requires IRAK4 and UNC93B1.** Sorted blood pDCs from mutated patients and healthy donors were cultured for 24 h with either medium or SARS-CoV-2. **(A)** Dot plot showing pDC diversification in P1, P2, and P3 subpopulations from magnetically sorted blood pDCs from homozygous IRAK4$^{-/-}$ ($n$ = 1), UNC93B1$^{-/-}$ ($n$ = 2), and TLR3$^{-/-}$ ($n$ = 1) donors, and sex- and age-matched healthy donors ($n$ = 2), were cultured for 24 h with either medium or SARS-CoV-2 at an MOI of 1. **(B)** Quantification of pro-inflammatory cytokines in the supernatant of activated pDCs for 24 h in response to SARS-CoV-2 challenge. Bars represent medians. HD, healthy donor; ND, not detectable.

TLR9 pathways, including IRAK4, MyD88, and UNC93B deficiencies.

Type I IFNs are critical cytokines to control viral replication. Several chronic viral infections were associated with poor type I IFN responses (Dolganiuc et al., 2006; Marsili et al., 2012; Lee et al., 2013; Snell et al., 2017). In COVID-19 patients, decreased serum levels of type I IFN were associated with severity in late-stage infection, and increased viral load (Tay et al., 2020; Acharya et al., 2020). Defective type I IFN immunity was shown to underlie life-threatening COVID-19 pneumonia in one of two ways, via inborn errors of TLR3- and IRF7-dependent type I IFN immunity (Zhang et al., 2020b) or via preexisting neutralizing auto-antibodies to type I IFN (Bastard et al., 2020). This raised the question of the cellular basis of critical COVID-19 in patients with defective type I IFN immunity (Zhang et al., 2020a). Indeed, type I IFN is produced by all cells of the human body, including pulmonary epithelial cells, which also respond to type I IFNs, while it can be produced at much higher levels by pDCs, which are the only cells expressing constitutively high levels of IRF7 (Liu, 2005).

The difficulty in designing current and future COVID-19 treatment strategies lies in part in the complexity of the host–virus interactions. Continued efforts in mapping and dissecting immune effector pathways to SARS-CoV-2 will be of major importance in order to design efficient treatment strategies adapted to each patient and stage of the infection.

## Materials and methods

### Patients

The experiments involving human subjects were conducted in accordance with local, national, and international regulations and were approved by the French Ethics Committee, the French National Agency for the Safety of Medicines and Health Products, and the French Ministry of Research (protocols C10-13 and C10-16). Informed consent was obtained from all patients included in this study.

The two patients with UNC93B1 deficiency suffered from two herpetic encephalitis episodes during childhood and are carrying homozygous mutations leading to a premature stop codon (1034del4) or an alternative splice event (781G>A; Casrouge et al., 2006). The TLR3-deficient patient also displayed herpetic encephalitis, and is carrying compound heterozygous mutations (P554S and E746X; Zhang et al., 2007; Guo et al., 2011). The IRAK4-deficient patient is a 5-yr-old female who presented cellulitis to *Staphylococcus aureus* and a neutropenia from the age of 2 yr and is carrying a homozygous stop-gain mutation (Q293X).

### pDC isolation and cell culture

Buffy coats from healthy human donors were obtained from Etablissement Français du Sang, Paris, Saint-Antoine Crozatier blood bank. PBMC were isolated through Ficoll density gradient centrifugation (Ficoll-Paque; GE Healthcare). pDCs were isolated through a first step of pDC magnetic sorting (Human Plasmacytoid DC Enrichment Kit; StemCell), and subsequent flow cytometric sorting on the basis of live, lineage$^-$ (CD16, CD14, CD19, CD20, CD56, and CD3), CD11c$^-$CD4$^+$, and CD2$^-$CD5$^-$ cells to a 98% purity. Due to some logistic issues, alternatively frozen PBMCs from Etablissement Français du Sang, Paris, Saint Louis blood bank, were thawed and placed at 37°C for 2 h for cell recovery. pDCs were then magnetically sorted (Human Plasmacytoid DC Enrichment Kit; StemCell). pDC enrichment was assessed based on the cytometric sorting panel, and ranged from 71 to 90%. African green monkey kidney epithelial Vero E6 cells (CRL-1586; ATCC) were cultured in Dulbecco's modified Eagle's medium (DMEM; Thermo Fisher Scientific) supplemented with 10% FBS, 1% penicillin-streptomycin, 1% GlutaMAX, and 25 mM Hepes.

### SARS-CoV-2 primary strain isolation and amplification

SARS-CoV-2 viruses were isolated from nasopharyngeal swab specimens collected at Service de Virologie (Hospital Saint Louis, Paris). Samples were centrifuged at 4,000 *g* for 10 min, then filtered using a 0.45-µM filter, and diluted 1:1 with DMEM-4% (DMEM supplemented with 4% FBS, 1% penicillin-streptomycin, 1% GlutaMAX, and 25 mM Hepes). Vero E6 cells were seeded in 96-well cell culture plates (15,000 cells/well) and incubated at 37°C with 200 µl of inoculum and observed daily for cytopathogenic effects by light microscopy. Substantial cytopathogenic effects were seen at 72–96 h after inoculation. Culture supernatants were then collected, clarified by centrifugation, filtered using a 0.45-µM filter, and kept at −80°C. We confirmed SARS-CoV-2 replication by RT-qPCR, and whole viral genome sequences were obtained by next-generation sequencing using Illumina MiSeq sequencers. Strain sequences have been deposited in the Global Initiative of Sharing All Influenza Data database under accession nos. EPI_ISL_469284 (220_95) and EPI_ISL_469283 (211_61). All viruses belong to the GH clade.

SARS-CoV-2 strains were further propagated on Vero E6 in DMEM-2% (DMEM supplemented with 2% FBS, 1% penicillin-streptomycin, 1% GlutaMAX, and 25 mM Hepes). Viruses were passaged three times before being used for experiments. For the last passage, viruses were purified through a 20% sucrose cushion by ultracentrifugation at 80,000 *g* for 2 h at 4°C. Pellets were resuspended in HNE 1×, pH 7.4 (Hepes 5 mM, NaCl 150 mM, and EDTA 0.1 mM), aliquoted, and stored at −80°C.

Virus titers were ascertained by plaque assays in Vero E6 cells and expressed as PFU per milliliter. Cells were incubated for 1 h with 10-fold dilution of viral stocks. The inoculum was then replaced with Avicel 2.4% mixed at an equal volume with DMEM supplemented with 4% FBS, 2% Glutamax, 50 mM $MgCl_2$, and 0.225% of $NaHCO_3$, and incubated 3 d at 37°C before plaque counting.

### Infection assays

Vero cells were plated (50,000 cell per well) in 24-well plates for 4 h before being incubated with SARS-CoV-2 diluted in DMEM-2%. Freshly purified pDCs were seeded in 96-well plates (50,000 cells per well) and incubated with SARS-CoV-2 diluted in pDC culture medium (RPMI 1640 medium with GlutaMAX, 10% of FBS, 1% of MEM nonessential amino acid, 1% of sodium pyruvate, and 1% of penicillin-streptomycin). At 2 h, 24 h, and 48 h after inoculation, Vero cells were trypsinized and transferred to 96-well plates. Vero and pDCs were washed with PBS and fixed with 2% (vol/vol) paraformaldehyde diluted in PBS for 15 min at room temperature. Cells were incubated for 1 h at 4°C with 1 µg/ml of anti-nucleoprotein mAb (40143-MM05; Sino Biological) diluted in permeabilization flow cytometry buffer (PBS supplemented with 5% FBS, 0.5% [wt/vol] saponin, and 0.1% sodium azide). After washing, cells were incubated with 1 µg/ml of Alexa Fluor 488 (115–545-003; Jackson ImmunoResearch) or 647-conjugated (115–606-062; Jackson ImmunoResearch) goat anti-mouse IgG diluted in permeabilization flow cytometry buffer for 30 min at 4°C. SARS-CoV-2 infection was quantified by flow cytometry.

To quantify infectious viral particles released in the supernatants of infected cells, pDCs and Vero cells were inoculated with SARS-CoV-2 as described above and incubated at 37°C for 72 h. At indicated time points, supernatants were collected and kept at −80°C. Virus titer was then determined by plaque assay on Vero E6 cells as described above.

### Kinetic of infection by qPCR assay

Vero E6 and pDCs were inoculated with SARS-CoV-2 as described above. At the indicated time points, cells were washed thrice with PBS. Vero E6 were further incubated with trypsin 0.25% for 5 min at 37°C to remove cell surface–bound particles. Total RNA was extracted using the RNeasy plus mini kit (Qiagen) according to the manufacturer's instructions. cDNAs were generated from 80 ng total RNA by using the Maxima First Strand Synthesis Kit following the manufacturer's instructions (Thermo Fisher Scientific). Amplification products were incubated with 1 U RNase H for 20 min at 37°C, followed by 10 min at 72°C for enzyme inactivation, and diluted 10-fold in DNase/RNase-free water. Real-time quantitative PCR was performed using a Power Syber Green PCR Master Mix (Thermo Fisher Scientific) on a Light Cycler 480 (Roche). The primers used for qPCR were E_Sarbeco_F1 (5′-ACAGGTACGTTAATAGTTAATAGCGT-3′) and E_Sarbeco_R2 (5′-ATATTGCAGCAGTACGCACACA-3′) for viral RNA quantification. The plasmid containing the sequence corresponding to the amplified cDNA was purchased from GenScript (pUC57-2019-nCoV-PC:E; MC_0101078) and serially diluted (294 to 2.94 × $10^9$ gene copies/µl) to generate standard curves.

### pDC activation

Freshly sorted pDCs were cultured in 96-well plates at a concentration of 5 × $10^5$ cells per milliliter in the presence of medium alone (RPMI 1640 medium with GlutaMAX, 10% of FBS, 1% of MEM nonessential amino acid, 1% of sodium pyruvate, and 1% of penicillin-streptomycin), Flu (2 µg/ml; A/PR/8/34l Charles River), or the SARS-CoV-2 primary strain 220_95 or 211_61 at an MOI of 1. For intracellular cytokine staining, SARS-CoV-2 was used at an MOI of 2 to activate pDCs. After 24 or 48 h of culture, pDC supernatant was collected and stored at −80°C for subsequent cytokine quantification. pDCs were stained for flow cytometry analysis.

### Flow cytometry analysis

To sort pDCs, cells were stained with zombie violet or Brilliant UltraViolet fixable viability dye (Biolegend), FITC anti-CD16 (clone NKP15; BD), FITC anti-CD14 (clone TÜK4; Miltenyi), FITC anti-CD19 (clone LT19; Miltenyi), FITC anti-CD20 (clone 2H7; BD), FITC anti-CD56 (clone HCD56; Biolegend), FITC anti-CD3 (clone HIT3a; BD), BV650 or AF700 anti-CD4 (clone OKT4; Biolegend), PE-Cy7 anti-CD11c (clone Bu15; Biolegend), APC-Vio770 anti-CD2 (clone LT2; Miltenyi), and APC anti-CD5 (clone UCHT2; BD). pDCs were gated as live, lineage$^-$ (CD16, CD14, CD19, CD20, CD56, and CD3), CD2$^-$CD5$^-$, and CD4$^+$CD11c$^-$ cells.

To detect intracellular cytokines, Brefeldin A Solution 1000X (eBioscience) was added to the wells 19 h after the beginning of the activation for 5 h. Cells were then fixed and permeabilized using the Intracellular Fixation and Permeabilization Buffer Set (eBioscience), and stained with IFNα-V450 (clone 7N4-1; BD) and TNF-α-APC (clone MAb11; BD).

For pDC diversification and checkpoint assessment, cells were stained with zombie violet fixable viability dye (Biolegend), BV711 anti-CD123 (clone 6H6; Biolegend), PE anti-CD80 (clone L307.4; BD), PerCP-efluor 710 anti-PD-L1 (clone MIH1; eBioscience), BUV737 anti-CD86 (clone 2331; BD), BV421 anti-OX40 Ligand (clone ik-1; BD), APC anti-CD62L (clone DREG-56; BD), and FITC anti-CCR7 (clone 150503; R&D Systems).

For ACE2 cell surface expression, the indicated cells were incubated with a goat anti-human ACE2 polyclonal antibody (5 µg/ml; AF933; Bio-Techne) in 100 µl of PBS with 0.02% $NaN_3$ and 5% FBS for 1 h at 4°C. Cells were then washed and incubated with an Alexa 647–conjugated secondary antibody (Jackson ImmunoResearch) for 30 min at 4°C.

Acquisition was performed on an Attune NxT Flow Cytometer (Thermo Fisher Scientific) or an LSR Fortessa (BD Biosciences), and analysis was done by using FlowJo software (Tree Star). Flow cytometry analyses were performed at the flow cytometry core facility of Institut de Recherche Saint-Louis (Paris, France).

### Secreted inflammatory cytokines measurement

pDC cytokine production of IFN-α2, IL-8, IL-6, IP-10, and TNF-α was measured in culture supernatants using a BD cytometric bead array according to the manufacturer's protocol, with a 20 pg/ml detection limit. Acquisitions were performed on a LSR Fortessa (BD Biosciences), and cytokine concentrations were determined using FCAP Array Software (BD Biosciences).

The concentration of secreted IFN-λ1 was measured by ELISA (DuoSet DY7246; R&D Systems) according to the manufacturer's instructions. The manufacturer reported neither cross-reactivity nor interference with IFN-α, IFN-β 1a, IL-10Rβ, IFN-λ2 and λ3, and IL-28Rα. The optical density (OD) value of the supernatants was defined as absolute OD value minus the OD absorbance from blank wells. The detection limit was 85 pg/ml, and all samples were run in duplicate.

### Statistical analysis

Statistical analyses were performed with one-way ANOVA, Kruskal–Wallis test with Dunn's multiple comparison post-test, or Mann–Whitney test, in Prism (GraphPad Software).

### Online supplemental material

Fig. S1, A and B, shows that magnetically sorted frozen pDC diversification is similar to FACS, fresh pDCs when activated with SARS-CoV-2 or Flu, demonstrating that the technical limitations we encountered during this work did not impact its relevance. Data shown in Fig. S1 C highlight pDC diversification when activated with either free SARS-CoV-2 or SARS-CoV-2–infected cells. Fig. S1, D and E, presents additional evidence from Fig. 1 that pDCs are not permissive to SARS-CoV-2 infection. Fig. S2 provides additional information on Figs. 1, 2, and 3. Fig. S2, A–C, shows pDC diversification and pro-inflammatory cytokines after 48 h of culture with medium, SARS-CoV-2, or Flu. Fig. S2, D and E, demonstrates that tonsillar pDCs can also undergo diversification and pro-inflammatory cytokine secretion when activated with Flu or SARS-CoV-2 compared with medium. Fig. S3, which relates to Fig. 4, shows HCQ potential to inhibit pDC diversification in a dose-dependent manner and demonstrates the absence of OX40L$^{high}$ pDCs when cultured with HCQ, providing further evidence that HCQ has inhibitory effects on pDC diversification.

## Acknowledgments

A. Amara dedicates this work to the memory of his colleagues and friends, Professor Jean-Louis Virelizier (Unité d'Immunologie Virale, Institut Pasteur, Paris) and Professor Renaud Mahieux (École Nationale Supérieure and Centre International de Recherche en Infectiologie, Lyon, France), who left us during the SARS-CoV-2 pandemic.

The authors thank Maud Salmona, Severine Mercier-Delarue, and Tiffanie Bouillé (Laboratoire de Virologie, Hôpital Saint Louis) for SARS-CoV-2 deep sequencing, Marie Laure Chaix (Laboratoire de Virologie, Hôpital Saint-Louis, Paris, France) for the nasopharyngeal swabs, and Lauriane Goldwirt (Laboratoire de Pharmacologie Biologique, Hôpital Saint-Louis, Paris, France) for providing us with HCQ. We warmly thank S. Boucherit for administrative assistance. The authors thank all the Personnel Soignant de l'Hôpital Saint-Louis for their amazing work during the COVID-19 pandemic.

A. Amara's laboratory received funding from the French Government's Investissement d'Avenir program, Laboratoire d'Excellence "Integrative Biology of Emerging Infectious Diseases" (grant ANR-10-LABX-62-IBEID), the Fondation pour la Recherche Médicale (grant FRM-EQU202003010193), the Agence Nationale de la Recherche (ANR-FRM FLASH COVID project IDISCOVR), and the Université de Paris (Plan de Soutien Covid-19: RACPL20FIR01-COVID-SOUL). V. Soumelis's team was supported by the Agence Nationale de la Recherche (ANR-17-CE15-0003, and ANR-17-CE15-0003-01) and by the Université de Paris "PLAN D'RGENCE COVID19." The Laboratory of Human Genetics of Infectious Diseases is supported by the Howard Hughes Medical Institute, Rockefeller University, the St. Giles Foundation, Institut National de la Santé et de la Recherche Médicale, Université de Paris, the French Foundation for Medical Research (EQU201903007798), the French National Research Agency under the "Investments for the Future" program (ANR-10-IAHU-01), the Integrative Biology of Emerging

Infectious Diseases Laboratory of Excellence (ANR-10-LABX-62-IBEID), the CNSVIRGEN project (ANR-18-CE15-0009-01), the SEAe-HostFactors project (ANR-18-CE15-0020-02), the National Institutes of Health (R01AI088364), the National Center for Advancing Translational Sciences, the National Institutes of Health Clinical and Translational Science Award program (UL1 TR001866), a Fast Grant from Emergent Ventures, the Mercatus Center at George Mason University, the Yale Center for Mendelian Genomics and the GSP Coordinating Center funded by the National Human Genome Research Institute (UM1HG006504 and U24HG008956), the French Foundation for Medical Research and French National Research Agency GENCOVID project (ANRS-COV05), the Square Foundation, the Fisher Center for Alzheimer's Research Foundation, and Grandir – Fonds de Solidarité pour l'Enfance.

Author contributions: A. Amara and V. Soumelis conceived the study. F. Onodi, L. Bonnet-Madin, A. Amara, and V. Soumelis designed the experiments. F. Onodi performed the pDC purification and FACS analysis with J. Poirot. L. Bonnet-Madin, and L. Meertens performed the virus strain isolation and the infection studies. F. Onodi and L. Karpf performed pDC purification and cytokine quantification. J.-M. Molina, C. Delaugerre, and J. Le Goff performed the sequencing of the SARS-CoV-2 strains. S.-Y. Zhang, A. Puel, E. Jouanguy, Q. Zhang, and J.-L. Casanova coordinated recruitment and provided patient samples. J.-L. Casanova revised the manuscript. C. Picard provided patient samples and collected clinical data. F. Onodi, A. Amara, and V. Soumelis wrote the initial manuscript draft, and all authors contributed to the final form of the manuscript.

Disclosures: J.-M. Molina reported grants from Gilead and personal fees from Merck, ViiV, and Janssen outside the submitted work. V. Soumelis reported grants from Sanofi and Roche, and personal fees from Leo Pharma, Gilead, Merck, and Sanofi outside the submitted work. No other disclosures were reported.

Submitted: 1 July 2020
Revised: 8 October 2020
Accepted: 7 January 2021

## References

Abe, M., and A.W. Thomson. 2006. Dexamethasone preferentially suppresses plasmacytoid dendritic cell differentiation and enhances their apoptotic death. *Clin. Immunol.* 118:300–306. https://doi.org/10.1016/j.clim.2005.09.019

Acharya, D., G. Liu, and M.U. Gack. 2020. Dysregulation of type I interferon responses in COVID-19. *Nat. Rev. Immunol.* 20:397–398. https://doi.org/10.1038/s41577-020-0346-x

Alculumbre, S.G., V. Saint-André, J. Di Domizio, P. Vargas, P. Sirven, P. Bost, M. Maurin, P. Maiuri, M. Wery, M.S. Roman, et al. 2018. Diversification of human plasmacytoid predendritic cells in response to a single stimulus. *Nat. Immunol.* 19:63–75. https://doi.org/10.1038/s41590-017-0012-z

Asselah, T., D. Durantel, E. Pasmant, G. Lau, and R.F. Schinazi. 2020. COVID-19: discovery, diagnostics and drug development. *J. Hepatol.* 0. https://doi.org/10.1016/j.jhep.2020.09.031

Bastard, P., L.B. Rosen, Q. Zhang, E. Michailidis, H.-H. Hoffmann, Y. Zhang, K. Dorgham, Q. Philippot, J. Rosain, V. Béziat, et al. 2020. Autoantibodies against type I IFNs in patients with life-threatening COVID-19. *Science.* 370:eabd4585. https://doi.org/10.1126/science.abd4585

Blackwell, S.E., and A.M. Krieg. 2003. CpG-A-induced monocyte IFN-gamma-inducible protein-10 production is regulated by plasmacytoid dendritic cell-derived IFN-alpha. *J. Immunol.* 170:4061–4068. https://doi.org/10.4049/jimmunol.170.8.4061

Bontkes, H.J., J.J. Ruizendaal, D. Kramer, C.J.L.M. Meijer, and E. Hooijberg. 2005. Plasmacytoid dendritic cells are present in cervical carcinoma and become activated by human papillomavirus type 16 virus-like particles. *Gynecol. Oncol.* 96:897–901. https://doi.org/10.1016/j.ygyno.2004.10.040

Casanova, J.-L., L. Abel, and L. Quintana-Murci. 2011. Human TLRs and IL-1Rs in host defense: natural insights from evolutionary, epidemiological, and clinical genetics. *Annu. Rev. Immunol.* 29:447–491. https://doi.org/10.1146/annurev-immunol-030409-101335

Casrouge, A., S.-Y. Zhang, C. Eidenschenk, E. Jouanguy, A. Puel, K. Yang, A. Alcais, C. Picard, N. Mahfoufi, N. Nicolas, et al. 2006. Herpes simplex virus encephalitis in human UNC-93B deficiency. *Science.* 314:308–312. https://doi.org/10.1126/science.1128346

Cervantes-Barragan, L., R. Züst, F. Weber, M. Spiegel, K.S. Lang, S. Akira, V. Thiel, and B. Ludewig. 2007. Control of coronavirus infection through plasmacytoid dendritic-cell-derived type I interferon. *Blood.* 109:1131–1137. https://doi.org/10.1182/blood-2006-05-023770

Cervantes-Barragan, L., K.L. Lewis, S. Firner, V. Thiel, S. Hugues, W. Reith, B. Ludewig, and B. Reizis. 2012. Plasmacytoid dendritic cells control T-cell response to chronic viral infection. *Proc. Natl. Acad. Sci. USA.* 109:3012–3017. https://doi.org/10.1073/pnas.1117359109

Ciancanelli, M.J., S.X.L. Huang, P. Luthra, H. Garner, Y. Itan, S. Volpi, F.G. Lafaille, C. Trouillet, M. Schmolke, R.A. Albrecht, et al. 2015. Infectious disease. Life-threatening influenza and impaired interferon amplification in human IRF7 deficiency. *Science.* 348:448–453. https://doi.org/10.1126/science.aaa1578

Corzo, C.A., E. Varfolomeev, A.F. Setiadi, R. Francis, S. Klabunde, K. Senger, S. Sujatha-Bhaskar, J. Drobnick, S. Do, E. Suto, et al. 2020. The kinase IRAK4 promotes endosomal TLR and immune complex signaling in B cells and plasmacytoid dendritic cells. *Sci. Signal.* 13:eaaz1053. https://doi.org/10.1126/scisignal.aaz1053

Das, S., S. Bhowmick, S. Tiwari, and S. Sen. 2020. An Updated Systematic Review of the Therapeutic Role of Hydroxychloroquine in Coronavirus Disease-19 (COVID-19). *Clin. Drug Investig.* 40:591–601. https://doi.org/10.1007/s40261-020-00927-1

Dolganiuc, A., S. Chang, K. Kodys, P. Mandrekar, G. Bakis, M. Cormier, and G. Szabo. 2006. Hepatitis C virus (HCV) core protein-induced, monocyte-mediated mechanisms of reduced IFN-alpha and plasmacytoid dendritic cell loss in chronic HCV infection. *J. Immunol.* 177:6758–6768. https://doi.org/10.4049/jimmunol.177.10.6758

Florentin, J., B. Aouar, C. Dental, C. Thumann, G. Firaguay, F. Gondois-Rey, V. Soumelis, T.F. Baumert, J.A. Nunès, D. Olive, et al. 2012. HCV glycoprotein E2 is a novel BDCA-2 ligand and acts as an inhibitor of IFN production by plasmacytoid dendritic cells. *Blood.* 120:4544–4551. https://doi.org/10.1182/blood-2012-02-413286

Frazão, J.B., P.R. Errante, and A. Condino-Neto. 2013. Toll-like receptors' pathway disturbances are associated with increased susceptibility to infections in humans. *Arch. Immunol. Ther. Exp. (Warsz.).* 61:427–443. https://doi.org/10.1007/s00005-013-0243-0

Gilliet, M., W. Cao, and Y.-J. Liu. 2008. Plasmacytoid dendritic cells: sensing nucleic acids in viral infection and autoimmune diseases. *Nat. Rev. Immunol.* 8:594–606. https://doi.org/10.1038/nri2358

Guermonprez, P., J. Valladeau, L. Zitvogel, C. Théry, and S. Amigorena. 2002. Antigen presentation and T cell stimulation by dendritic cells. *Annu. Rev. Immunol.* 20:621–667. https://doi.org/10.1146/annurev.immunol.20.100301.064828

Guo, Y., M. Audry, M. Ciancanelli, L. Alsina, J. Azevedo, M. Herman, E. Anguiano, V. Sancho-Shimizu, L. Lorenzo, E. Pauwels, et al. 2011. Herpes simplex virus encephalitis in a patient with complete TLR3 deficiency: TLR3 is otherwise redundant in protective immunity. *J. Exp. Med.* 208:2083–2098. https://doi.org/10.1084/jem.20101568

Hirsch, I., C. Caux, U. Hasan, N. Bendriss-Vermare, and D. Olive. 2010. Impaired Toll-like receptor 7 and 9 signaling: from chronic viral infections to cancer. *Trends Immunol.* 31:391–397. https://doi.org/10.1016/j.it.2010.07.004

Hjorton, K., N. Hagberg, E. Israelsson, L. Jinton, O. Berggren, J.K. Sandling, K. Thörn, J. Mo, M.-L. Eloranta, and L. Rönnblom. DISSECT consortium. 2018. Cytokine production by activated plasmacytoid dendritic cells and natural killer cells is suppressed by an IRAK4 inhibitor. *Arthritis Res. Ther.* 20:238. https://doi.org/10.1186/s13075-018-1702-0

Hoffmann, M., H. Kleine-Weber, S. Schroeder, N. Krüger, T. Herrler, S. Erichsen, T.S. Schiergens, G. Herrler, N.-H. Wu, A. Nitsche, et al. 2020. SARS-CoV-2 Cell Entry Depends on ACE2 and TMPRSS2 and Is Blocked by a Clinically Proven Protease Inhibitor. *Cell.* 181:271–280.e8. https://doi.org/10.1016/j.cell.2020.02.052

Keni, R., A. Alexander, P.G. Nayak, J. Mudgal, and K. Nandakumar. 2020. COVID-19: Emergence, Spread, Possible Treatments, and Global Burden. *Front. Public Health.* 8:216. https://doi.org/10.3389/fpubh.2020.00216

Lee, B.L., and G.M. Barton. 2014. Trafficking of endosomal Toll-like receptors. *Trends Cell Biol.* 24:360–369. https://doi.org/10.1016/j.tcb.2013.12.002

Lee, M.S., C.H. Park, Y.H. Jeong, Y.-J. Kim, and S.-J. Ha. 2013. Negative regulation of type I IFN expression by OASL1 permits chronic viral infection and CD8$^+$ T-cell exhaustion. *PLoS Pathog.* 9:e1003478. https://doi.org/10.1371/journal.ppat.1003478

Lepelletier, Y., R. Zollinger, C. Ghirelli, F. Raynaud, R. Hadj-Slimane, A. Cappuccio, O. Hermine, Y.-J. Liu, and V. Soumelis. 2010. Toll-like receptor control of glucocorticoid-induced apoptosis in human plasmacytoid predendritic cells (pDCs). *Blood.* 116:3389–3397. https://doi.org/10.1182/blood-2010-05-282913

Liu, Y.-J. 2005. IPC: professional type 1 interferon-producing cells and plasmacytoid dendritic cell precursors. *Annu. Rev. Immunol.* 23:275–306. https://doi.org/10.1146/annurev.immunol.23.021704.115633

Marsili, G., A.L. Remoli, M. Sgarbanti, E. Perrotti, A. Fragale, and A. Battistini. 2012. HIV-1, interferon and the interferon regulatory factor system: an interplay between induction, antiviral responses and viral evasion. *Cytokine Growth Factor Rev.* 23:255–270. https://doi.org/10.1016/j.cytogfr.2012.06.001

Meera, S., T. Madhuri, G. Manisha, and P. Ramesh. 2010. Irreversible loss of pDCs by apoptosis during early HIV infection may be a critical determinant of immune dysfunction. *Viral Immunol.* 23:241–249. https://doi.org/10.1089/vim.2009.0112

Meyers, J.H., J.S. Justement, C.W. Hallahan, E.T. Blair, Y.A. Sun, M.A. O'Shea, G. Roby, S. Kottilil, S. Moir, C.M. Kovacs, et al. 2007. Impact of HIV on cell survival and antiviral activity of plasmacytoid dendritic cells. *PLoS One.* 2:e458. https://doi.org/10.1371/journal.pone.0000458

Picard, C., A. Puel, M. Bonnet, C.-L. Ku, J. Bustamante, K. Yang, C. Soudais, S. Dupuis, J. Feinberg, C. Fieschi, et al. 2003. Pyogenic bacterial infections in humans with IRAK-4 deficiency. *Science.* 299:2076–2079. https://doi.org/10.1126/science.1081902

Raj, V.S., S.L. Smits, L.B. Provacia, J.M.A. van den Brand, L. Wiersma, W.J.D. Ouwendijk, T.M. Bestebroer, M.I. Spronken, G. van Amerongen, P.J.M. Rottier, et al. 2014. Adenosine deaminase acts as a natural antagonist for dipeptidyl peptidase 4-mediated entry of the Middle East respiratory syndrome coronavirus. *J. Virol.* 88:1834–1838. https://doi.org/10.1128/JVI.02935-13

Rothenfusser, S., E. Tuma, S. Endres, and G. Hartmann. 2002. Plasmacytoid dendritic cells: the key to CpG. *Hum. Immunol.* 63:1111–1119. https://doi.org/10.1016/S0198-8859(02)00749-8

Sacre, K., L.A. Criswell, and J.M. McCune. 2012. Hydroxychloroquine is associated with impaired interferon-alpha and tumor necrosis factor-alpha production by plasmacytoid dendritic cells in systemic lupus erythematosus. *Arthritis Res. Ther.* 14:R155. https://doi.org/10.1186/ar3895

Scheuplein, V.A., J. Seifried, A.H. Malczyk, L. Miller, L. Höcker, J. Vergara-Alert, O. Dolnik, F. Zielecki, B. Becker, I. Spreitzer, et al. 2015. High secretion of interferons by human plasmacytoid dendritic cells upon recognition of Middle East respiratory syndrome coronavirus. *J. Virol.* 89:3859–3869. https://doi.org/10.1128/JVI.03607-14

Snell, L.M., T.L. McGaha, and D.G. Brooks. 2017. Type I Interferon in Chronic Virus Infection and Cancer. *Trends Immunol.* 38:542–557. https://doi.org/10.1016/j.it.2017.05.005

Soumelis, V., I. Scott, F. Gheyas, D. Bouhour, G. Cozon, L. Cotte, L. Huang, J.A. Levy, and Y.J. Liu. 2001. Depletion of circulating natural type 1 interferon-producing cells in HIV-infected AIDS patients. *Blood.* 98:906–912. https://doi.org/10.1182/blood.V98.4.906

Tang, D., P. Comish, and R. Kang. 2020. The hallmarks of COVID-19 disease. *PLoS Pathog.* 16:e1008536. https://doi.org/10.1371/journal.ppat.1008536

Tay, M.Z., C.M. Poh, L. Rénia, P.A. MacAry, and L.F.P. Ng. 2020. The trinity of COVID-19: immunity, inflammation and intervention. *Nat. Rev. Immunol.* 20:363–374. https://doi.org/10.1038/s41577-020-0311-8

Thomas, J.M., Z. Pos, J. Reinboth, R.Y. Wang, E. Wang, G.M. Frank, P. Lusso, G. Trinchieri, H.J. Alter, F.M. Marincola, and E. Thomas. 2014. Differential responses of plasmacytoid dendritic cells to influenza virus and distinct viral pathogens. *J. Virol.* 88:10758–10766. https://doi.org/10.1128/JVI.01501-14

van der Made, C.I., A. Simons, J. Schuurs-Hoeijmakers, G. van den Heuvel, T. Mantere, S. Kersten, R.C. van Deuren, M. Steehouwer, S.V. van Reijmersdal, M. Jaeger, et al. 2020. Presence of Genetic Variants Among Young Men With Severe COVID-19. *JAMA.* 324:663. https://doi.org/10.1001/jama.2020.13719

Villani, A.-C., R. Satija, G. Reynolds, S. Sarkizova, K. Shekhar, J. Fletcher, M. Griesbeck, A. Butler, S. Zheng, S. Lazo, et al. 2017. Single-cell RNA-seq reveals new types of human blood dendritic cells, monocytes, and progenitors. *Science.* 356:eaah4573. https://doi.org/10.1126/science.aah4573

World Health Organization. 2020. Weekly epidemiological update - 24 November 2020. https://www.who.int/publications/m/item/weekly-epidemiological-update—24-november-2020.

Zhang, S.-Y., E. Jouanguy, S. Ugolini, A. Smahi, G. Elain, P. Romero, D. Segal, V. Sancho-Shimizu, L. Lorenzo, A. Puel, et al. 2007. TLR3 deficiency in patients with herpes simplex encephalitis. *Science.* 317:1522–1527. https://doi.org/10.1126/science.1139522

Zhang, Q., P. Bastard, A. Bolze, E. Jouanguy, S.Y. Zhang, A. Cobat, L.D. Notarangelo, H.C. Su, L. Abel, and J.L. Casanova. COVID Human Genetic Effort. 2020a. Life-Threatening COVID-19: Defective Interferons Unleash Excessive Inflammation. *Med (N Y).* 1:14–20. https://doi.org/10.1126/science.abd4570

Zhang, Q., P. Bastard, Z. Liu, J. Le Pen, M. Moncada-Velez, J. Chen, M. Ogishi, I.K.D. Sabli, S. Hodeib, C. Korol, et al. NIAID-USUHS/TAGC COVID Immunity Group. 2020b. Inborn errors of type I IFN immunity in patients with life-threatening COVID-19. *Science.* 370:eabd4570. https://doi.org/10.1126/science.abd4570

# Supplemental material

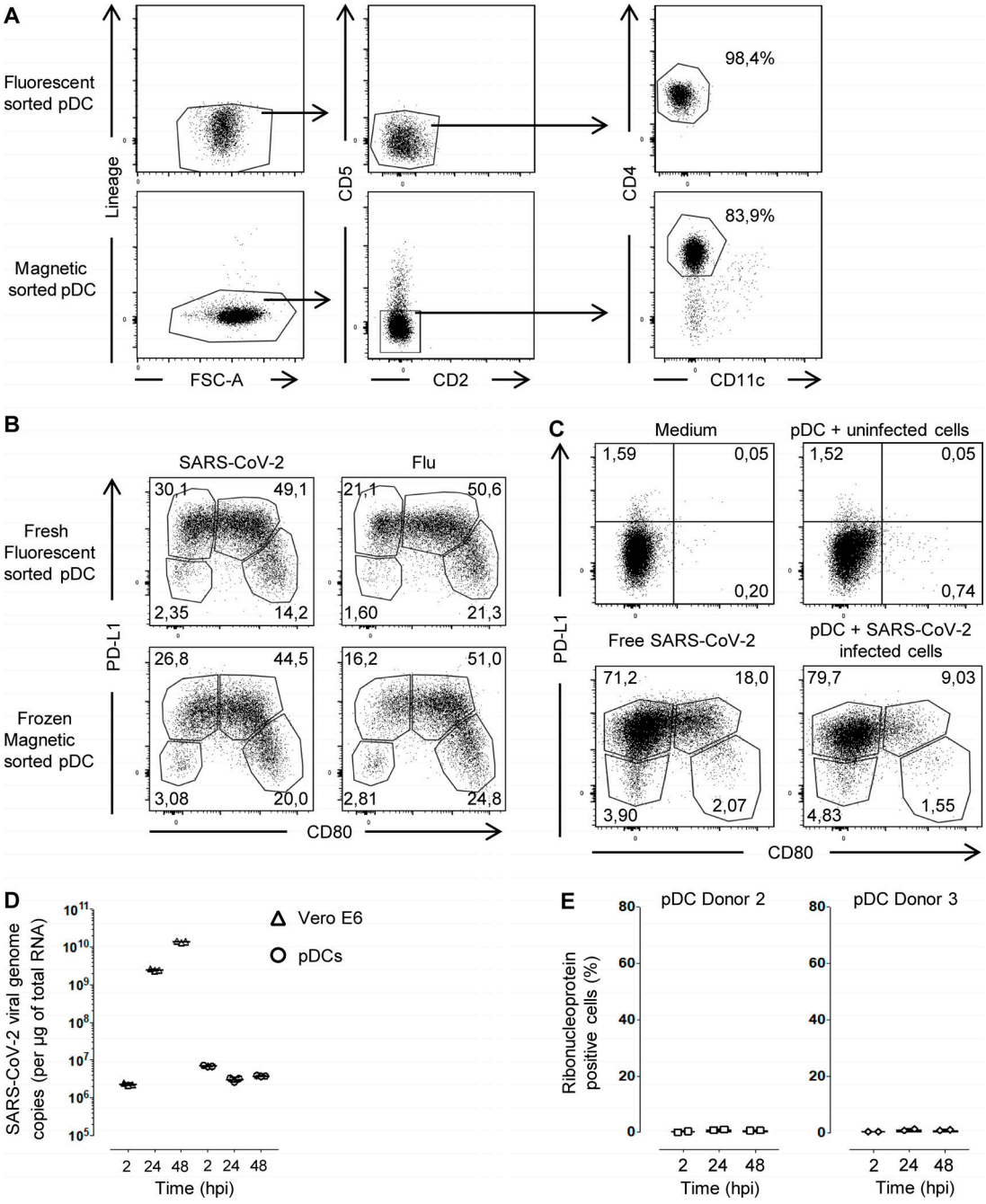


Figure S1. **SARS-CoV-2 induces pDC activation.** Sorted blood pDCs from healthy donors were cultured for 24 h with medium, SARS-CoV-2, or Flu. **(A)** Percentage of pure pDCs among live cells through different sorting strategies. Results from two healthy donors representative of $n = 8$. **(B)** P1, P2, and P3 diversification of fresh, fluorescent-sorted pDCs versus frozen, magnetic-sorted pDCs with either SARS-CoV-2 or Flu for 24 h. Results from two healthy donors representative of $n = 8$. **(C)** Dot plot of pDC activation with either free SARS-CoV-2 or pDC co-culture with SARS-CoV-2–infected cells. Results from $n = 1$ healthy donors. **(D)** Viral RNA copy number of Vero E6 and pDCs 2, 24, and 48 h post-infection (hpi). Results from one experiment representative of $n = 3$. **(E)** Intracellular production of the nucleoprotein antigen (N) on pDCs of two healthy donors of $n = 3$. FSC-A, forward scatter area.

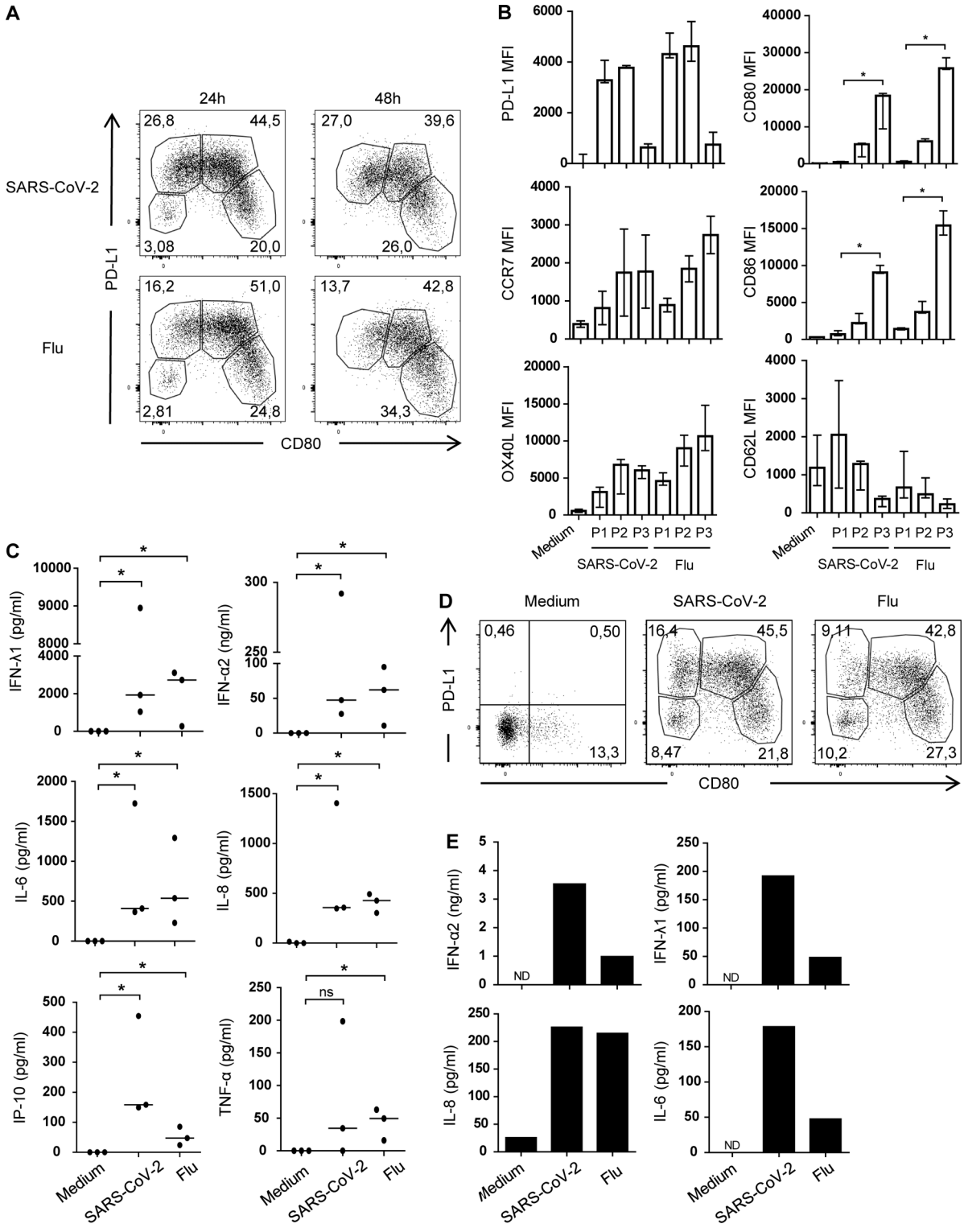


Figure S2. **SARS-CoV-2 induces activation and diversification of tonsilar pDCs.** Sorted blood pDCs from healthy donors were cultured for 48 h with medium, SARS-CoV-2, or Flu. **(A)** Dot plot showing pDC activation and diversification through the expression of PD-L1 and CD80 at 24 h and 48 h. Results from one healthy donor representative of $n = 3$. **(B)** Geometric mean (mean fluorescence intensity [MFI]) of pDCs' activation markers at 48 h. Histograms represent medians and bars interquartile ranges of $n = 3$ healthy donors from three independent experiments. **(C)** Quantification of secreted pro-inflammatory cytokines 48 h after culture. Bars represent medians of $n = 3$ healthy donors from three independent experiments. **(D)** Dot plot of tonsil pDC activation cultured for 24 h with medium, SARS-CoV-2, or Flu. Results from $n = 1$ healthy donors. **(E)** Quantification of pro-inflammatory cytokines of tonsilar pDCs at 24 h. Histograms represent medians of $n = 1$ healthy donor. *, $P < 0.05$; Kruskal–Wallis with Dunn's multiple comparisons post-test (B); Mann–Whitney test (C). ND, not detectable; ns, not significant.

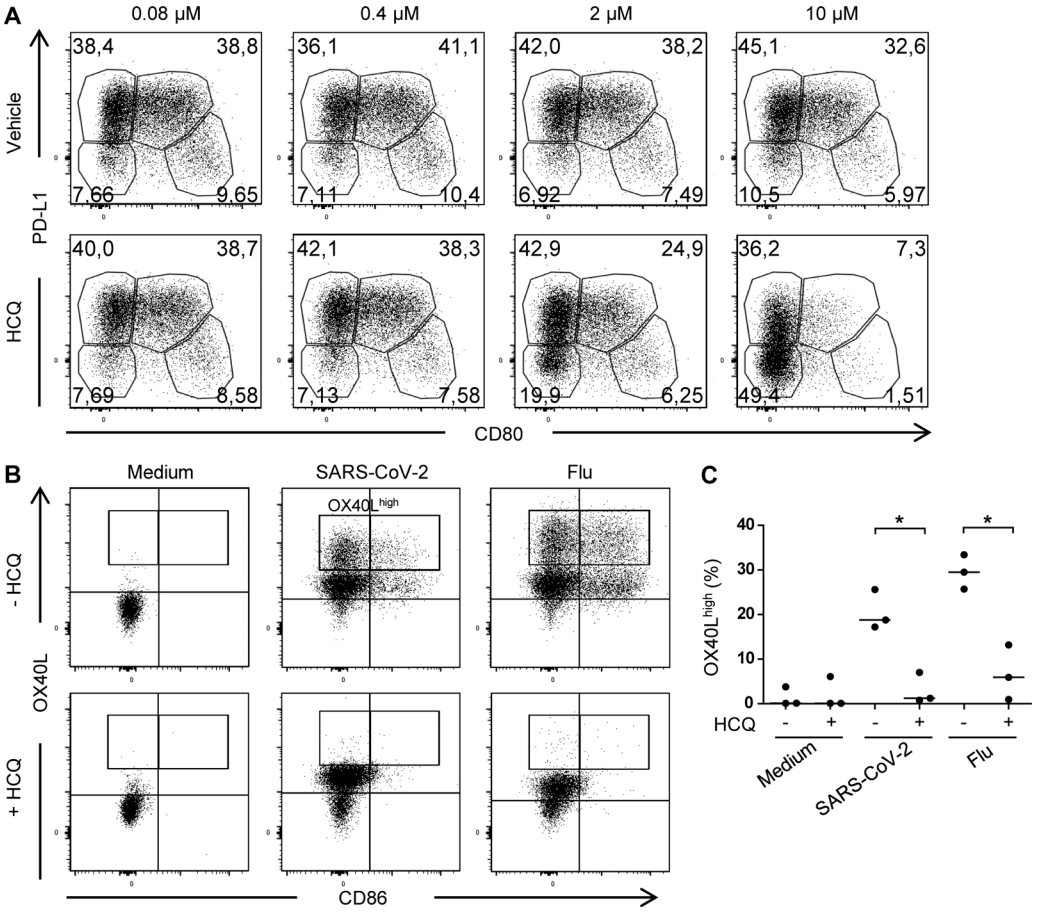


Figure S3. **HCQ inhibits SARS-CoV-2–induced pDC activation in a dose-dependent manner.** Sorted blood pDCs from healthy donors were cultured for 24 h with medium, Flu, or SARS-CoV-2 at an MOI of 1 with HCQ or vehicle. **(A)** Dot plot of pDC diversification with increasing concentration of HCQ or vehicle. Results from one healthy donor representative of $n = 3$. **(B)** Dot plot showing OX40L and CD86 in the presence or absence of HCQ. Results from one healthy donor representative of $n = 3$. **(C)** Percentage of $OX40L^{high}$ population among pDCs. Bars represent medians of $n = 3$ healthy donors from three independent experiments. *, $P < 0.05$; Mann–Whitney test.